Two-Color Surface Plasmon Polariton Enhanced Upconversion in NaYF4:Yb:Tm Nanoparticles on Au Nanopillar Arrays

ARTICLE *in* THE JOURNAL OF PHYSICAL CHEMISTRY C · FEBRUARY 2014

Impact Factor: 4.77 · DOI: 10.1021/jp4115173

10 AUTHORS, INCLUDING:

Sheng Liu
Sandia National Laboratories
57 PUBLICATIONS **251** CITATIONS
SEE PROFILE

Ting S. Luk
Sandia National Laboratories
208 PUBLICATIONS **3,353** CITATIONS
SEE PROFILE

Mahdi Farrokh Baroughi
South Dakota State University
71 PUBLICATIONS **291** CITATIONS
SEE PROFILE

Steve J. Smith
South Dakota School of Mines and Technology
68 PUBLICATIONS **793** CITATIONS
SEE PROFILE

THE JOURNAL OF PHYSICAL CHEMISTRY C

Article

pubs.acs.org/JPCC

Two-Color Surface Plasmon Polariton Enhanced Upconversion in $NaYF_4$:Yb:Tm Nanoparticles on Au Nanopillar Arrays

QuocAnh Luu,[†,‡,⊥] Amy Hor,[†,⊥] Jon Fisher,[†] Robert B. Anderson,[†] Sheng Liu,[§] Ting-Shan Luk,[§] Hari P. Paudel,[#] Mahdi Farrokh Baroughi,[#] P. Stanley May,*[,‡] and Steve Smith*[,†]

[†]Nanoscience and Nanoengineering, South Dakota School of Mines and Technology, Rapid City, South Dakota 57701, United States

[‡]Chemistry Department, University of South Dakota, Vermillion, South Dakota 57069, United States

[§]Center for Integrated Nanotechnologies, Sandia National Laboratories, Albuquerque, New Mexico 87123, United States

[#]Electrical Engineering and Computer Science Department, South Dakota State University, Brookings, South Dakota 57007, United States

ABSTRACT: Spectroscopic imaging and time-resolved spectroscopy are used to study the surface plasmon polariton (SPP) enhanced infrared to visible upconversion luminescence from $NaYF_4$:Tm:Yb nanoparticles embedded in polymethyl methylacrylate (PMMA) supported on Au nanopillar arrays. The arrays have a lattice resonance associated with the SPP near 980 nm, near-resonant with the peak absorption of the Yb^{3+} ion, while a local surface plasmon resonance (LSPR) associated with the individual pillars is seen to enhance the near-infrared emission of Tm^{3+} ions near 780 nm. The two combined channels of enhancement result in a significantly higher enhancement of the near-infrared emission when compared to the visible upconversion lines of the Tm^{3+} ion, consistent with the interpretation of sequential surface plasmon assisted absorption and emission at two separate and disparate energies. The presence of SPP and LSPR was confirmed by spectrally resolved reflectivity, and the mechanisms for luminescence enhancement were further confirmed by time-resolved measurements of the upconversion luminescence.

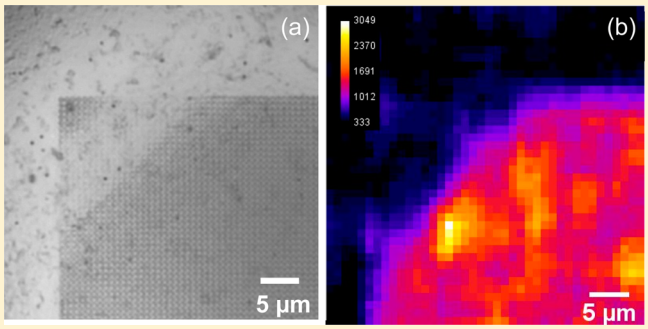

INTRODUCTION

While the majority of luminescent materials emit light at longer wavelengths compared to the excitation source, there are many technological applications that can benefit from atypical materials that convert lower energy photons into higher energy photons, a process known as upconversion (UC). While upconversion can be achieved through a variety of optical processes, such as two-photon absorption, second-harmonic generation, cooperative luminescence, two-step absorption, and energy transfer upconversion, at low excitation intensity, the energy transfer upconversion process is by far the most efficient.[1] With the advent of nanosized UC materials, the range of applications wherein such materials can be deployed has greatly increased. For instance, the areas of bioimaging, biolabeling, and photodynamic therapy benefit greatly from upconverting nanoparticle (UCNP) materials due to the long penetration depth of near-infrared light in biological tissues and the minimization of undesired background fluorescence from the NIR excitation.[2,3] Thus, a great deal of effort has been recently focused on improving this class of materials.

The most extensively explored UCNPs are Ln^{3+}-doped β-$NaYF_4$ nanocrystals, particularly with Yb^{3+} as the sensitizer, and Er^{3+} or Tm^{3+} as the activator.[4,5] These particles are very efficient upconverters, as their constituent ions have more than one long-lived metastable level, a prerequisite for the energy transfer UC process, and high intrinsic quantum efficiency due to the shielding of the f-orbitals from the environment.[1] However, the high intrinsic quantum efficiency of the emitting states in upconversion nanoparticles is offset by the poor external quantum efficiency due to the low absorption coefficient of lanthanides.[1,6]

Driven by the novel applications of UC, enhancement of the UC process has been widely investigated. One of the primary methods is through the introduction of metallic surfaces or nanostructures, as metal−fluorophore interactions are known to modify the kinetics of nearby fluorophores. In the vicinity of a metallic nanostructure, luminescence enhancement can be achieved through the amplification of the incident field, where local electromagnetic fields at the UCNP position are intensified due to plasmon resonances, and through the modification of the radiative rates of the phosphors.[7−11] By optimizing the geometry of the metallic nanostructures, and placing them within suitable proximity to the UCNPs, significant enhancement in UC efficiency should be achievable.

Received: November 22, 2013
Revised: January 20, 2014

   dx.doi.org/10.1021/jp4115173 | J. Phys. Chem. C XXXX, XXX, XXX−XXX

In this regard, there have been many reports of enhancement of the UC efficiencies through metal coupling to lanthanide-doped materials, such as Er^{3+}- and Pr^{3+}-doped glasses embedded with Ag nanoparticles,[12−14] and β-$NaYF_4$:Er^{3+}, Yb^{3+} coupled with Ag and Au nanostructures.[11,15,16]

These previous studies have primarily focused on coupling a surface plasmon resonance to either the infrared absorption or visible upconverted emission bands of these phosphors. However, because of the unusually large energy separation between the absorbing and emitting states inherent to the upconversion process, a unique opportunity exists to engineer metallic nanostructures that simultaneously, and independently, influence both emission and absorption. In the present study, we utilize the collective modes of a nanopillar array to effect enhanced infrared absorption and simultaneously exploit the localized resonances associated with the individual pillars to enhance select lines in the upconverted emission from β-$NaYF_4$:0.3% Tm^{3+}, 25% Yb^{3+} nanoparticles. It is demonstrated that a significant increase in total upconversion luminescence yield can be achieved with this approach, herein referred to as two-color surface plasmon polariton (SPP) assisted upconversion. Using spectroscopic imaging, the effect is illustrated by comparing the luminescence enhancement from β-$NaYF_4$:0.3% Tm^{3+}, 25% Yb^{3+} nanoparticles embedded in polymethyl methylacrylate (PMMA) films supported on either a smooth Au surface (control) or neighboring Au nanopillar arrays. The mechanisms are further clarified by time-resolved measurements of the time dependence of the upconverted luminescence following pulsed NIR excitation.

EXPERIMENTAL METHODS

Fabrication of Au Nanopillar Arrays. The gold nanopillar arrays were constructed using an electron beam lithography technique. The silicon substrate was cleaned using RCA-I cleaning procedure. Prior to the gold deposition, chromium was used as an adhesion layer. Ten nanometers of chromium and 100 nm of gold were deposited on the cleaned silicon substrate using a Torr combination rf sputtering system. A 300 nm thick film of electron beam resist (495 PMMA polymers with 6% solid in anisole) was spin-coated onto the gold surface at 4000 rpm for 45 s and then heated on a hot plate for 1 min at 180 °C. Photoresist was exposed to electron-beam dose of 350 μC/cm^2, from a Hitachi scanning electron microscope (S-3400N) equipped with an NPGS nanopattering accessory, to make a 100 × 100 μm^2 squared pattern. The pattern was developed in methyl isobutyl ketone (MIBK)/isopropanol (IPA):1/3 solution, purchased from Microchem, for 25 s. A 70 nm gold layer was deposited above the patterned surface using a CHA e-Beam evaporator. The PMMA mask was removed by immersing the substrate in a Remover PG solution for 4 h at room temperature to reveal the 100 × 100 μm^2 gold nanopillars patterned area.

Synthesis of β-$NaYF_4$:0.3% Tm^{3+}, 25% Yb^{3+} Nanoparticles. Ytterbium oxide and thulium oxide were obtained from Trona. Yttrium oxide (99.9%), oleic acid (90%), 1-octadecane (90%), and poly(methyl methacrylate) were obtained from Alfa Aesar. Acetic acid (glacial, 99.9%) was from Pharm Co. Sodium fluoride (>99%) was obtained from Fischer Scientific.

The blue upconverting nanoparticles, UCNPs, were synthesized using the method of Lin et al.[17] and was comprised of β-$NaYF_4$:0.3% Tm^{3+}, 25% Yb^{3+} with oleic acid as a capping agent. The precursor pot contained 0.5 mmol of lanthanide oleate solution (74.7% yttrium, 25% ytterbium, and 0.3% thulium) that was prepared from 0.374 mmol of $Y(CH_3COO)_3$, 0.125 mmol of $Yb(CH_3COO)_3$, and 0.0015 mmol of $Tm(CH_3COO)_3$ in 50% v/v acetic acid/water reacting with 6 mL of oleic acid. The solution was heated at 100 °C under a vacuum for 1 h until the precursor solution turned clear.

The second pot was the fluoride solution, which contained 0.5 mmol of sodium acetate and 2 mmol of sodium fluoride, dissolved in 10 mL of 1-octadecene and 2 mL of oleic acid. This mixture was heated to 100 °C under a vacuum for 30 min and then ramped to 315 °C with a gentle stream of nitrogen gas and the vacuum closed off. The precursor solution was injected into the fluoride solution within a few seconds to ensure a narrow size distribution of upconversion nanoparticles. The reaction was maintained at 320 °C for 30 min.

The nanoparticles were cleaned from the excess oleic acid by precipitating the nanoparticles out of the solution with acetone, centrifuged at 5000 rpm, and then dispersed in toluene. The cleaning process was repeated at least three times until a white solid was obtained.

Deposition of Thin Films of β-$NaYF_4$:0.3% Tm:25% Er Nanoparticles Embedded in PMMA. For the preparation of PMMA films, 100 mg of PMMA and 100 mg of upconversion nanoparticles were dissolved in 2 mL of toluene and 10 mL of chloroform. The solution was sonicated for 1 h before being spin-coated onto the gold engineered surfaces. The gold engineered surfaces were spun at 3500 rpm before releasing one drop of PMMA solution containing upconversion nanoparticles.

Spectroscopic Imaging System. Confocal upconversion luminescence images were obtained using a custom-built confocal microscopy system. The system is comprised of a high numerical aperture objective lens (Olympus UMPlanFl 100×, NA = 0.95) and a 980 nm CW diode laser (Thorlabs) operating at 1.1 mW for the excitation and collection of the emission from the sample in an epi-illumination mode. The estimated power excitation intensity is ≈100 kW/cm^2. The 980 nm excitation laser was directed through a dichroic mirror toward the sample, and the resultant upconverted emission light passed through the dichroic mirror (separating the excitation light) into a 0.64 m single grating spectrometer (150 lines/mm, Jobin Yvon HR640), where the resultant spectra were imaged by the CCD (Princeton Instruments SPEC-10). The sample was raster scanned using a computer-controlled piezoelectric stage, and spectra at every pixel were collected to form a spectrally resolved two-dimensional image.

Time-Resolved Spectroscopy Measurements. For the time-resolved spectroscopy measurements, an optical parametric oscillator (OPO) pulsed-laser (Opolette by Opotek) was used in place of the diode laser as the excitation source. A lens with a focal length of approximately 32 cm was added between the two mirrors to expand the laser beam to increase the spot size and reduce the incident intensity. The objective lens used was an Olympus UMPlanFl 10×, NA = 0.3. The pulse laser was operated at 11 mW. A Hamamatsu R928 photomultiplier tube (PMT) operated at 1.2 kV, mounted laterally on the spectrometer, was used in combination with an SR-430 multichannel scaler (SR 430) for photon counting.

RESULTS AND DISCUSSION

UCNPs of β-$NaYF_4$:0.3% Tm^{3+}, 25% Yb^{3+} were synthesized in the Chemistry Department at the University of South Dakota, as described in the Experimental Methods and an earlier

dx.doi.org/10.1021/jp4115173 | J. Phys. Chem. C XXXX, XXX, XXX−XXX

publication.[17] The UC process in these materials is described by the energy level diagram shown in Figure 1. Yb^{3+} acts as a

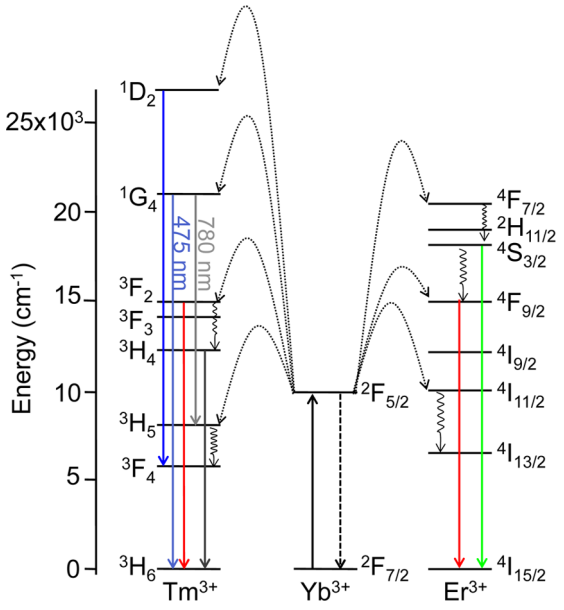

Figure 1. Energy level diagram showing the upconversion mechanism of $NaYF_4$:Tm:Yb and $NaYF_4$:Er:Yb.

sensitizer that absorbs the 980 nm NIR excitation light via the $^2F_{7/2} \rightarrow {}^2F_{5/2}$ transition. Subsequent multiple, consecutive energy transfers from Yb^{3+} to the activator Tm^{3+} ion are responsible for the upconversion emission. NIR excitation at 980 nm produces blue luminescence at 450 and 475 nm, corresponding to the $^1D_2 \rightarrow {}^3F_4$ and $^1G_4 \rightarrow {}^3H_6$ transitions, red luminescence at 647 nm corresponding to the $^3F_2 \rightarrow {}^3H_6$ transition, and NIR luminescence at 780 and 800 nm corresponding to the $^1G_4 \rightarrow {}^3H_5$ and $^3H_4 \rightarrow {}^3H_6$ transitions, respectively.[18,19]

Figure 2a shows a TEM image of a thin film of the 60−80 nm diameter β-$NaYF_4$:0.3% Tm^{3+}, 25% Yb^{3+} nanoparticles used in this study, embedded in a 100 nm thick PMMA film. Figure 2b shows an AFM image of the Au nanopillar arrays used in this study, which were specifically designed to fulfill the momentum mismatch between the wave vector of the incident light field and the SPP near-resonant with the Yb^{3+} absorption at 980 nm, the design details of which were previously reported.[20,21] Briefly, the Au nanopillars are 310 nm in diameter and 70 nm in height, with a periodic spacing of 620 nm. Four 100 × 100 μm^2 patterned areas were constructed on a silicon substrate coated with a 100 nm thick Au film. A thin film of PMMA (approximately 100 nm thick as determined from AFM) containing the β-$NaYF_4$:0.3% Tm^{3+}, 25% Yb^{3+} UCNPs was then spin-coated onto the substrate. A schematic of the sample is as shown in Figure 2c.

Spectrally resolved reflectivity measurements were made of the Au nanopillar arrays to verify the SPP absorption resonances using a home-built white-light reflectivity apparatus accessed through Sandia National Laboratories' Center for Integrated Nanotechnologies (CINT), the infrared portion of the spectrum was independently confirmed using two different Fourier transform infrared (FTIR) microscope systems, at Sandia National Laboratories and the National Renewable Energy Laboratory, with results similar to our earlier publication using similar nanostructured substrates.[16] The measurement results shown in Figure 3 confirm the presence

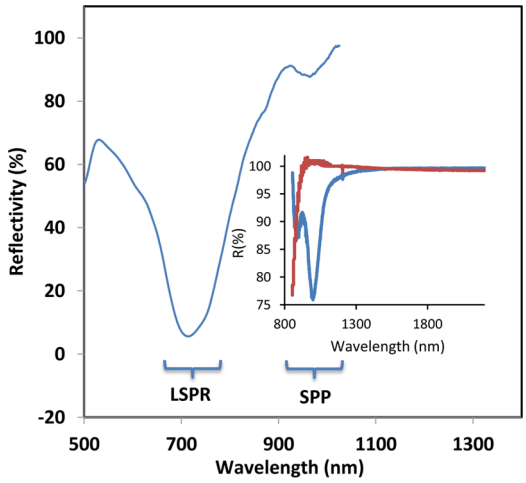

Figure 3. Visible broadband reflectivity spectra of the Au nanopillar array illustrating the presence of a local surface plasmon resonance (LSPR) and the surface plasmon polariton (SPP) appearing at approximately 980 nm, near-resonant with the Yb^{3+} absorption (also measured with an FTIR microscope as shown in the inset: blue curve, reflectivity of array, red curve, reflectivity of nearby unpatterened Au surface, from ref 16).

of the SPP near-resonant with the Yb^{3+} ion absorption at approximately 980 nm, but the visible reflectivity measurements also shows a broad absorption centered near approximately 750 nm, also confirmed by finite difference time domain (FDTD) simulations,[22] which we attribute to a localized surface plasmon resonance (LSPR), as has been reported previously for similar metallic nanostructures.[23,24] This broad feature in the reflectivity appears near-resonant with the NIR emission lines of Tm^{3+} near 780−800 nm, and we postulated that additional enhancement in the emission channel for this system may be achievable. To test this assertion, nanopillar arrays were prepared with thin films of PMMA embedded with our β-

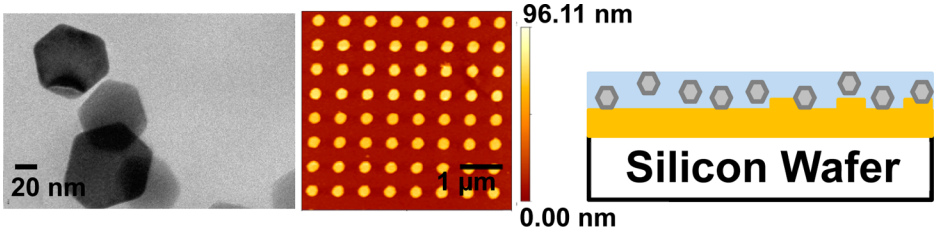

Figure 2. (a) TEM image of the β-$NaYF_4$:0.3% Tm^{3+}, 25% Yb^{3+} nanoparticles in PMMA; (b) AFM image of Au nanopillar array;[16] and (c) schematic drawing of the sample showing nanoparticles embedded in PMMA on continuous Au surface and Au patterned area of sample.

dx.doi.org/10.1021/jp4115173 | J. Phys. Chem. C XXXX, XXX, XXX−XXX

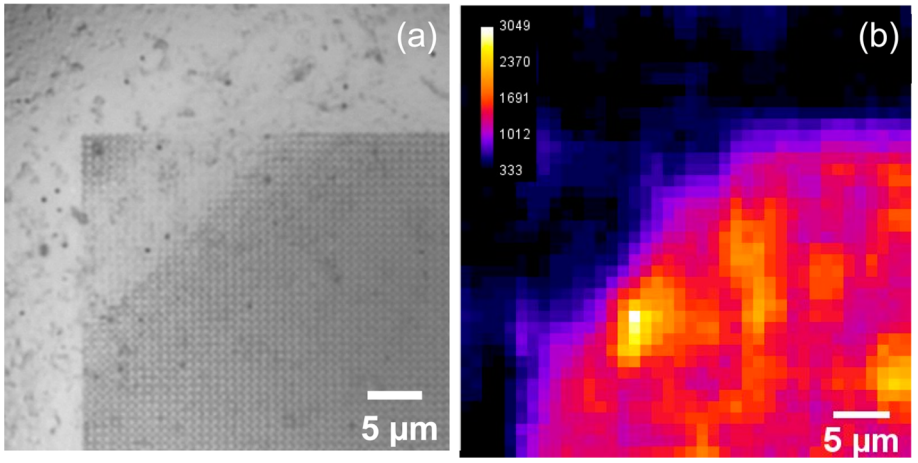

Figure 4. (a) Bright field optical image, and (b) intensity map of the β-$NaYF_4$:0.3% Tm^{3+}, 25% Yb^{3+} on a smooth Au surface and Au nanopillar array formed from the spectrally resolved data at λ = 780 nm.

$NaYF_4$:0.3% Tm^{3+}, 25% Yb^{3+} UCNPs, as shown in Figure 2, and spectroscopic imaging was performed near the borders of the nanopillar arrays and the neighboring unpatterned Au substrates.

Figure 4a shows a bright field optical image of the area of interest, showing both the smooth Au surface and the Au patterned area, each coated with the β-$NaYF_4$:0.3% Tm^{3+}, 25% Yb^{3+} nanoparticles embedded in PMMA. This same area was raster-scanned using a computer-controlled piezoelectric stage and a custom-built confocal microscope (see Experimental Methods) to produce a two-dimensional luminescence image shown in Figure 4b. From the confocal image, the area with the Au nanopillars is distinctively brighter compared to the smooth Au surface. The upconversion luminescence spectra of the blue, red, and NIR transitions, taken from the smooth Au surface and the Au patterned area, are overlaid in Figure 5a.

As can be seen in Figure 5, the NIR emission bands generally appear stronger compared to the visible emission, and as discussed below, experience a greater relative enhancement. In the low power limit, only one NIR emission peak has been reported for Tm^{3+} at approximately 800 nm, assigned to the $^3H_4 \rightarrow {}^3H_6$ transition.[5] However, previous authors reported that at a power density of 100 W/cm^2 to 1.3 kW/cm^2, additional peaks start to form around the main 800 nm peak.[25−27] Because of the very tight focusing used here, we estimate an excitation power density of ∼100 kW/cm^2 and also observe additional NIR emission bands in the neighborhood of 800 nm, that is, the very prominent peak near 780 nm, assigned to the $^1G_4 \rightarrow {}^3H_5$ transition.[18]

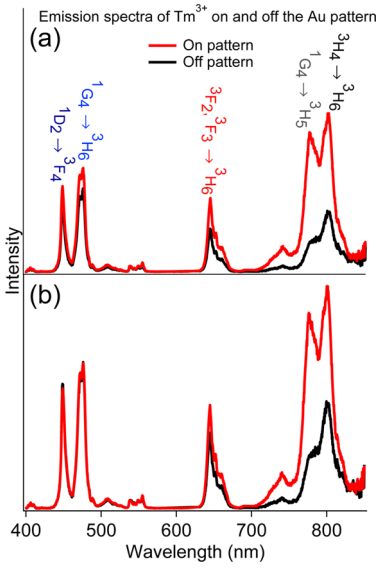

Figure 5. (a) Overlay of the upconversion luminescence spectra taken on and off the Au patterned area and (b) luminescence spectra normalized to 475 nm transition.

Statistical analysis of the upconversion luminescence images was performed to obtain the average intensity enhancement factor for each transition, derived by comparing the intensity between the patterned and unpatterned areas. Intensity histograms of all pixels in the images obtained were generated. The upconversion luminescence enhancement was calculated by obtaining the ratio of the two peaks which appear in the histograms (representing the average intensity on the smooth Au surface and Au patterned area, respectively), and the uncertainties were calculated from the full width at half-maximum of the respective peaks in the histograms. The widths of these histograms are attributed to variations in particle density and orientation. Visible luminescence of blue (450 and 475 nm transitions) and red (647 nm transition) show approximately 1.5× and 2.4× enhancement, respectively, whereas significantly higher enhancement was observed for both the 780 and 800 nm transitions in the NIR region, approximately 5.5×. These results are summarized in Table 1. We note here that both the 475 and 780 nm transitions originate from the same emitting state ($^1G_4$), and as such, the

Table 1. Luminescence Enhancement Ratio at Select Wavelengths[a]

transition	luminescence enhancement
450 nm	1.48 ± 0.28
475 nm	1.08 ± 0.89
647 nm	2.37 ± 0.35
780 nm	5.57 ± 0.85
800 nm	5.50 ± 0.97

[a]Ratio of the intensity of the Au patterned area relative to the smooth Au surface at each transition of the β-$NaYF_4$:0.3% Tm^{3+}, 25% Yb^{3+} sample.

dx.doi.org/10.1021/jp4115173 | J. Phys. Chem. C XXXX, XXX, XXX−XXX

observed variations in enhancement factor must be independent of the population of this state. We therefore interpret the significantly greater enhancement at 780 nm as strong evidence of radiative control via coupling to a surface plasmon resonance associated with the nanopillar substrate.[9,28] This point is further illustrated by normalizing the emission spectra to the intensity of the 475 nm emission as shown in Figure 5b.

The Au nanopillar array was specifically designed to fulfill the momentum mismatch between the wave vector of the incident light field and the SPP near the Yb^{3+} absorption resonance at 980 nm. We have previously shown that the enhancement of the visible upconversion luminescence lines of β-$NaYF_4$:3% Er^{3+}, 17% Yb^{3+} on Au nanopillar patterned substrates was due to the plasmonic properties of the nanostructured substrate.[16] Similarly, the enhancement of the visible upconversion luminescence at 450, 475, and 647 nm observed for β-$NaYF_4$:0.3% Tm^{3+}, 25% Yb^{3+} nanoparticles supported on identical Au patterned substrates is attributed to the interaction of the Yb^{3+} ions with the SPP resonant near 980 nm. However, the larger enhancement observed in the NIR region suggests an additional enhancement channel, which we attribute to the broad LSPR centered near 750 nm which selectively enhances the emission of the transitions near 780−800 nm. We propose the combined effects of the SPP at 980 nm and the broad LSPR near 750 nm result in a higher upconversion luminescence enhancement of the NIR emission as compared to the visible emission. Further evidence of the effect was revealed through time-resolved measurements of the upconversion luminescence decay.

Time-resolved spectroscopy measurements of the upconversion luminescence from β-$NaYF_4$:0.3% Tm^{3+}, 25% Yb^{3+} samples were taken on the Au patterned area and the smooth Au surface, for the 647 nm and 780−800 nm transitions, respectively, using an OPO and a multichannel scaler. The resultant upconversion luminescence decay curves are depicted in Figure 6. Data were fit to the two component exponential function shown in eq 1.

$$f(t) = A(e^{-k_1 t} - e^{-k_2 t}) \quad (1)$$

In the equation above, $f(t)$ is the emission intensity, A is a scaling factor, and k_1 and k_2 are the rate constants for the decay and rise, respectively. The equation describes the time dependence of emission from a state that is fed from another state. Although the equation is empirical, the rate constants can be used to correlate changes in the upconversion kinetics with the observed intensity changes.

Table 2 summarizes the rate constants for the rise and decay of the β-$NaYF_4$:0.3% Tm^{3+}, 25% Yb^{3+} nanoparticles embedded in PMMA on both the smooth and patterned Au areas of the sample for the 647 nm and 780−800 nm transitions. The rate constants for the β-$NaYF_4$:3% Er^{3+}, 17% Yb^{3+} upconverting nanoparticles on smooth and patterned Au areas of an identical substrate at 647 nm is included for comparison. Time-resolved measurement for the β-$NaYF_4$:3% Er^{3+}, 17% Yb^{3+} on nanopillar arrays was not reported previously. The rise and decay of the time-resolved upconversion luminescence curve represent the excitation and the emission of the upconverting nanoparticles, respectively.

As the SPP-assisted absorption of Yb^{3+} near 980 nm is presumed to enhance all emission lines, the faster rise observed for all transitions (647 nm and 780−800 nm) for both β-$NaYF_4$:0.3% Tm^{3+}, 25% Yb^{3+} and β-$NaYF_4$:3% Er^{3+}, 17% Yb^{3+} nanoparticles on the Au patterned area is attributed to an SPP-assisted absorption process, which is identical for both varieties of nanoparticles (Yb^{3+} absorption). As shown in Table 2, the rate constant was approximately 1.4× to 1.5× faster on the patterned areas as compared to the smooth Au surface. However, for the decay rate, only the 780−800 nm transition of β-$NaYF_4$:0.3% Tm^{3+}, 25% Yb^{3+} is significantly changed. Its decay rate constant on the Au patterned area is approximately 1.52× that observed on the smooth Au surface. There was no significant change in the decay rate for the 647 nm transition for either β-$NaYF_4$:0.3% Tm^{3+}, 25% Yb^{3+} or β-$NaYF_4$:3% Er^{3+}, 17% Yb^{3+} nanoparticle samples when comparing emission from the smooth and patterned Au surfaces. Furthermore, this observation is consistent with the time integrated upconversion luminescence (Figure 5), which exhibited a more pronounced enhancement in the NIR region of the spectrum compared to the visible regions. Both measurements support the model of an SPP-assisted absorption of the infrared excitation at 980 nm, and a LSPR-assisted emission which is most pronounced in the NIR portions of the spectrum.

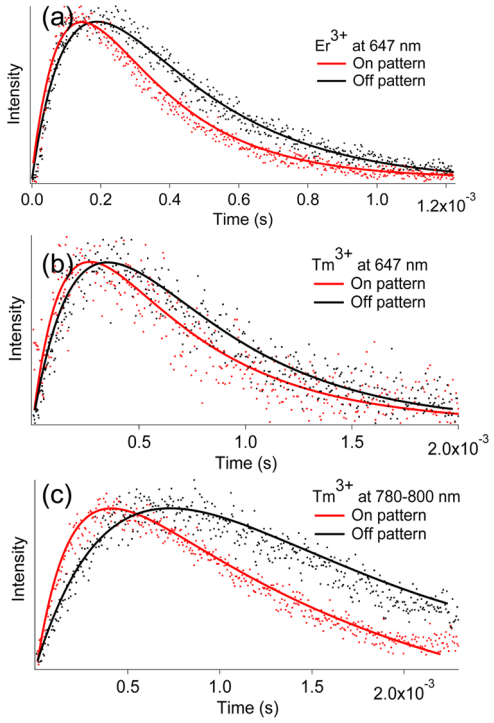

Figure 6. Upconversion luminescence decay on smooth Au surface (black) and the Au nanopillar array (red) for the $NaYF_4$:Er:Yb sample at (a) 647 nm and $NaYF_4$:Tm:Yb sample at (b) 647 nm and (c) 780−800 nm. Dots represent actual data, and the smooth curves represent the fit to the data.

CONCLUSIONS

In summary, the large energy separation between absorption and emission in the upconversion process lends itself to the possibility of compounding the effects of surface plasmon assisted absorption and emission at two disparate energies. The possibility of such control is a unique feature of the upconversion process and opens up possibilities for both fundamental studies and potential applications wherein absorption and emission processes need to be controlled separately and independently. We demonstrate here a nanopillar array is one plasmonic nanostructure whose design can be tailored to have surface plasmon resonances that coincide with

dx.doi.org/10.1021/jp4115173 | J. Phys. Chem. C XXXX, XXX, XXX−XXX

Table 2. Rate Constants for Upconverted Luminescence[a]

		smooth Au surface		Au patterned area		ratio	
sample	wavelength	rise	decay	rise	decay	rise	decay
$NaYF_4$:Er:Yb	647 nm	10353 ± 224	3464 ± 52	15736 ± 325	3785 ± 47	1.52 ± 0.04	1.09 ± 0.03
$NaYF_4$:Tm:Yb	647 nm	4029 ± 301	1927 ± 126	6100 ± 410	1909 ± 94	1.51 ± 0.14	0.99 ± 0.11
$NaYF_4$:Tm:Yb	800 nm	1662 ± 337	1097 ± 227	2372 ± 239	1664 ± 158	1.43 ± 0.30	1.52 ± 0.30

[a]The rate constants, in units of s^{-1}, for the rise and decay of both β-$NaYF_4$:0.3% Tm^{3+}, 25% Yb^{3+} and β-$NaYF_4$:3% Er^{3+}, 17% Yb^{3+} on the smooth and patterned Au surface and their corresponding ratios.

a lanthanide-based energy transfer upconversion system's absorption and emission energies. With further refinement, or development of new nanostructures with specified properties, significant improvements in upconversion enhancement may be possible, leading to more efficient upconverters, thereby enabling many of the technological applications of these materials.

AUTHOR INFORMATION

Corresponding Authors

*E-mail: (S.S.) Steve_Smith@mailaps.org.
*E-mail: (S.M.) Smay@usd.edu.

Author Contributions

[⊥]Q.L. and A.H. contributed equally. Imaging and time-resolved experiments were by Q.L. and A.H., spectrally resolved reflectivity and time-resolved data were contributed by J.F., R.A., S.L., and T.S.L., nanopillar arrays were designed and developed by H.P. and M.B., and P.S.M. and S.S. directed the work and wrote the manuscript. All authors have given approval to the final version of the manuscript.

Notes

The authors declare no competing financial interest.

ACKNOWLEDGMENTS

The authors acknowledge support from NSF (EPS-0903804, DGE-0903685, CHE-0840507) and the State of South Dakota, Governor's Office of Economic Development. P.S.M. acknowledges support from NASA (Cooperative Agreement Number: NNX10AN34A). The authors acknowledge Lynn Gedvilas of NREL for making the FTIR reflectivity measurements, Sandia National Laboratories for access to their facilities for reflectivity measurements, made under our CINT Proposal No. C2011B87, and the Nanofabrication Center at the University of Minnesota for providing access to the electron beam lithography and thermal evaporation systems.

REFERENCES

(1) Auzel, F. Upconversion and Anti-Stokes Processes with f and d Ions in Solids. *Chem. Rev.* **2004**, *104*, 139−173.
(2) Wang, F.; Banerjee, D.; Liu, Y.; Chen, X.; Liu, X. Upconversion Nanoparticles in Biological Labeling, Imaging, and Therapy. *Analyst* **2010**, *135*, 1839−1854.
(3) Zhang, P.; Steelant, W.; Kumar, M.; Scholfield, M. Versatile Photosensitizers for Photodynamic Therapy at Infrared Excitation. *J. Am. Chem. Soc.* **2007**, *129*, 4526−4527.
(4) Kra, K. W.; Biner, D.; Frei, G.; Gu, H. U.; Hehlen, M. P.; Lu, S. R. Hexagonal Sodium Yttrium Fluoride Based Green and Blue Emitting Upconversion Phosphors. *Chem. Mater.* **2004**, *28*, 1244−1251.
(5) Suyver, J. F.; Aebischer, a.; Biner, D.; Gerner, P.; Grimm, J.; Heer, S.; Krämer, K. W.; Reinhard, C.; Güdel, H. U. Novel Materials Doped with Trivalent Lanthanides and Transition Metal Ions Showing Near-Infrared to Visible Photon Upconversion. *Opt. Mater. (Amst).* **2005**, *27*, 1111−1130.
(6) Chen, D.; Wang, Y.; Hong, M. Lanthanide Nanomaterials with Photon Management Characteristics for Photovoltaic Application. *Nano Energy* **2012**, *1*, 73−90.
(7) Moskovits, M. Surface-Enhanced Spectroscopy. *Rev. Mod. Phys.* **1985**, *57*, 783.
(8) Lakowicz, J. R. Radiative Decay Engineering: Biophysical and Biomedical Applications. *Anal. Biochem.* **2001**, *298*, 1−24.
(9) Lakowicz, J. R. Radiative Decay Engineering 5: Metal-Enhanced Fluorescence and Plasmon Emission. *Anal. Biochem.* **2005**, *337*, 171−194.
(10) Esteban, R.; Laroche, M.; Greffet, J.-J. Influence of Metallic Nanoparticles on Upconversion Processes. *J. Appl. Phys.* **2009**, *105*, 033107.
(11) Schietinger, S.; Aichele, T.; Wang, H.-Q.; Nann, T.; Benson, O. Plasmon-Enhanced Upconversion in Single NaYF4:Yb^{3+}/Er^{3+} Co-doped Nanocrystals. *Nano Lett.* **2010**, *10*, 134−138.
(12) Da Silva, D. M.; Kassab, L. R. P.; Lüthi, S. R.; de Araújo, C. B.; Gomes, A. S. L.; Bell, M. J. V. Frequency Upconversion in Er^{3+} Doped PbO−GeO_2 Glasses Containing Metallic Nanoparticles. *Appl. Phys. Lett.* **2007**, *90*, 081913.
(13) Kassab, L. R. P.; de Araújo, C. B.; Kobayashi, R. a.; de Almeida Pinto, R.; da Silva, D. M. Influence of Silver Nanoparticles in the Luminescence Efficiency of Pr^{3+}-Doped Tellurite Glasses. *J. Appl. Phys.* **2007**, *102*, 103515.
(14) Rai, V. K.; Menezes, L. D. S.; de Araújo, C. B.; Kassab, L. R. P.; da Silva, D. M.; Kobayashi, R. A. Surface-Plasmon-Enhanced Frequency Upconversion in Pr^{3+} Doped Tellurium-Oxide Glasses Containing Silver Nanoparticles. *J. Appl. Phys.* **2008**, *103*, 093526.
(15) Feng, W.; Sun, L.-D.; Yan, C.-H. Ag Nanowires Enhanced Upconversion Emission of NaYF4:Yb,Er Nanocrystals via a Direct Assembly Method. *Chem. Commun. (Cambridge).* **2009**, 4393−4395.
(16) Paudel, H. P.; Zhong, L.; Bayat, K.; Baroughi, M. F.; Smith, S.; Lin, C.; Jiang, C.; Berry, M. T.; May, P. S. Enhancement of Near-Infrared-to-Visible Upconversion Luminescence Using Engineered Plasmonic Gold Surfaces. *J. Phys. Chem. C* **2011**, *115*, 19028−19036.
(17) Lin, C.; Berry, M. T.; Anderson, R.; Smith, S.; May, P. S. Highly Luminescent NIR-to-Visible Upconversion Thin Films and Monoliths Requiring No High-Temperature Treatment. *Chem. Mater.* **2009**, *21*, 3406−3413.
(18) Ye, S.; Zhu, B.; Luo, J.; Chen, J.; Lakshminarayana, G.; Qiu, J. Enhanced Cooperative Quantum Cutting in Tm^{3+}- Yb^{3+} Codoped Glass Ceramics Containing LaF_3 Nanocrystals. *Opt. Express* **2008**, *16*, 8989−8994.
(19) Suyver, J. F.; Grimm, J.; van Veen, M. K.; Biner, D.; Krämer, K. W.; Güdel, H. U. Upconversion Spectroscopy and Properties of $NaYF_4$ Doped with Er^{3+}, Tm^{3+} and/or Yb^{3+}. *J. Lumin.* **2006**, *117*, 1−12.
(20) Paudel, H. P.; Farrokh Baroughi, M.; Bayat, K. Plasmon Resonance Modes in Two-Dimensional Arrays of Metallic Nanopillars. *J. Opt. Soc. Am. B* **2010**, *27*, 1693.
(21) Paudel, H. P.; Bayat, K.; Baroughi, M. F.; May, S.; Galipeau, D. W. Geometry Dependence of Field Enhancement in 2D Metallic Photonic Crystals. *Opt. Express* **2009**, *17*, 22179−22189.
(22) Anderson, R. B.; Fisher, J.; Hor, A.; Lu, A.; Paudel, H.; Bayat, K.; Baroughi, M.; Luk, T.-S.; May, P. S.; Smith, S. Spectroscopic Imaging of Metal-Enhanced Upconversion on Plasmonic Substrates. *MRS Online Proc. Libr.* **2012**, *1457*, kk11−34.
(23) Auguié, B.; Barnes, W. Collective Resonances in Gold Nanoparticle Arrays. *Phys. Rev. Lett.* **2008**, *101*, 1−4.

(24) Song, J.-H.; Atay, T.; Shi, S.; Urabe, H.; Nurmikko, A. V. Large Enhancement of Fluorescence Efficiency from CdSe/ZnS Quantum Dots Induced by Resonant Coupling to Spatially Controlled Surface Plasmons. *Nano Lett.* **2005**, *5*, 1557−1561.
(25) Boyer, J.-C.; Vetrone, F.; Cuccia, L. a; Capobianco, J. a. Synthesis of Colloidal Upconverting $NaYF_4$ Nanocrystals Doped with Er^{3+}, Yb^{3+} and Tm^{3+}, Yb^{3+} via Thermal Decomposition of Lanthanide Trifluoroacetate Precursors. *J. Am. Chem. Soc.* **2006**, *128*, 7444−7445.
(26) Boyer, J.-C.; Cuccia, L. A.; Capobianco, J. A. Synthesis of Colloidal Upconverting NaYF4: Er^{3+} and Tm^{3+}/Yb^{3+} Monodisperse Nanocrystals. *Nano Lett.* **2007**, *7*, 847−852.
(27) Wang, F.; Liu, X. Upconversion Multicolor Fine-Tuning: Visible to Near-Infrared Emission from Lanthanide-Doped $NaYF_4$ Nanoparticles. *J. Am. Chem. Soc.* **2008**, *130*, 5642−5643.
(28) Barnes, W. L. Fluorescence Near Interfaces: the Role of Photonic Mode Density. *J. Mod. Opt.* **1998**, *45*, 661−669.